Supporting Information for: Electric Field Enhancements and Hot Spots in Amorphous Carbon Materials

Pablo Grobas Illobre,[†] Giorgio Conter,[‡] Luca Bonatti,[†] Tommaso Giovannini,[*,¶] Alessandro Fortunelli,[*,‡] and Chiara Cappelli[*,†]

†*Scuola Normale Superiore, Piazza dei Cavalieri 7, 56126 Pisa, Italy.*

‡*Institute of Chemistry of OrganoMetallic Compounds, Consiglio Nazionale delle Ricerche (CNR-ICCOM), Via Giovanni Moruzzi 1, Pisa 56124, Italy*

¶*Department of Physics and INFN, University of Rome Tor Vergata, Via della Ricerca Scientifica, 1, Rome, 00133, Italy*

E-mail: tommaso.giovannini@uniroma2.it; alessandro.fortunelli@cnr.it; chiara.cappelli@sns.it

S1 DynReaxMas a-C structures

S1.1 Massaged parameters and MM*n*/MM*m* notation

Within the DynReaxMas protocol, the PES exploration is accelerated by *massages*, that is, by judicious modifications of the ReaxFF potential parameters (including bond strengths, dispersion, bending constants, ...). Clearly, not all the massages affect the generation of the models in the same way (we refer to Ref. 1 for a more detailed discussion). On the one hand, a subset of parameters, the *hard* parameters, which include bond strengths, lead to a major reorganization of the structure (large displacement on the PES), which can be quantified by means of the root mean square displacement of the atoms. On the other hand, other parameters, the *soft* ones, allow for a more local exploration of the PES, helping to find the most stable configurations. In order to obtain structurally different models, it is thus important to always include at least one hard parameter in the massage sequence, but only at the beginning of the sequence, while allowing for a reconstruction of the networks under the massage of soft parameters in the following steps, especially the final ones. For this reason, we found it convenient in designing the DynReaxMas protocol to generate random sequences of 4 massages each, to be combined in pairs, one sequence containing at least 1 hard parameter massage, and one sequence that does not contain hard parameter massages. For instance, in the original DynReaxMas paper,[1] MM1 (for convenience here named M1) is a sequence of four massages including a hard parameter. M1 can be combined with MM8 (or M8), containing soft-only massages, to yield a MM1/MM8 DynReaxMas standardized massage protocol (or M18 for simplicity). Analogously, M3, containing massage of hard parameters, can be combined with M4, containing only soft massages, to give a proper MM3/MM4 DynReaxMas sequence or standardized massage protocol. In this work we simplify the notation from MM1/MM8 to M18.

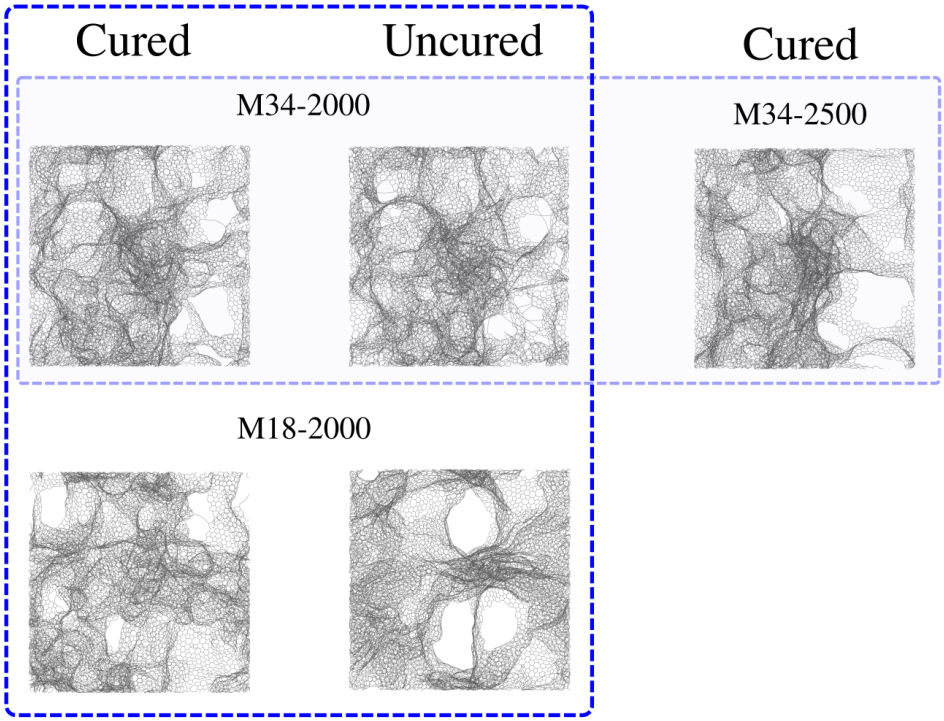

Figure S1: Schematic atomistic depiction of the different a-Carbon phases in their simulated unit cells.

S1.2 Main descriptors of a-C structures

Table S1 contains the main structural descriptors of the a-Carbon phases described in the main text. C1, C2, C3, C4, are the number of carbon atoms that have only one, two, three, four, respectively, neighbors within bonding distance, normalized by the total number of atoms in the cell. Pure graphene would have C1=C2=C4=0 and C3=1. As expected, the curing protocol increases the C3 content, which is related to the higher degree of graphitization achieved upon curing. A(sp) quantifies the deviation from the theoretical 180° angle energy minimum for 2-coordinated C atoms. Since the edges of the graphitic sheets have 2-coordinated atoms with 120° angles, smaller values of A(sp) in the cured phases are related to a higher sheet extension/edge ratio. R5, R6, R7 describe the number of 5-, 6-, and 7-member rings, respectively, as a percent (normalized by the total number of atoms). For reference, graphite would have R6=50, since every atom is part of three 6-member rings, so the total number of rings normalized by the number of atoms n is $3n/6n \times 100\% = 50$. It is apparent that the curing step increases the amount of 6-member rings while decreasing the 5-member ones.

In order to estimate the defect content of the structures (dangling bonds and/or unsaturation), we developed in Ref. 2 a screening probe protocol in which a mildly reactive molecule (a fake water-like species with

purposedly decreased overcoordination penalty) is introduced in the system to react with the defects. While we refer to the original work for details, Table S2 summarizes the percent number of atoms (normalized by the total amount of carbon atoms) that react with the probe. We note that the curing step clearly decreases the number of such sites, indicating a lower amount of high energy defects in the structures.

Table S1: Structural descriptors for the M18 and M34 phases discussed in the paper, in both their as-prepared and cured forms.

Structure	**C1**	**C2**	**C3**	**C4**	**A(sp)**	**R5**	**R6**	**R7**
050-18-2000cured	0.000	0.039	0.954	0.006	27.709	9.822	26.225	9.499
050-18-2000	0.000	0.092	0.892	0.016	22.929	11.135	18.894	9.363
050-34-2000cured	0.000	0.042	0.951	0.007	28.056	9.399	26.345	9.255
050-34-2000	0.000	0.093	0.884	0.022	21.084	10.461	19.975	9.559
050-34-2500cured	0.000	0.025	0.969	0.007	27.965	9.179	27.826	9.279
050-34-2500	0.000	0.040	0.943	0.017	24.688	9.782	24.118	9.714

Table S2: Percent number of sites vs. total number of carbon atoms that are available for saturation with a reactive water probe for the phases discussed in this paper, for both as-prepared and cured forms.

Structure	**Reacted**	**Structure**	**Reacted**
050-18-2000	16.46	050-18-2000 cured	13.58
050-34-2000	15.94	050-34-2000 cured	12.96
050-34-2500	12.50	050-34-2500 cured	11.17

S2 ωFQ parameters and dependence of the optical response on τ

Table S3: ωFQ parameters exploited in the calculations.[3]

Parameter	Value
η	0.37 a.u.
τ	170.0 a.u.
E_F	0.4 eV
$\mathscr{A}_i$	0.4879 Å^2
d	100.0
s	1.2
l_{ij}^0	1.4129 Å

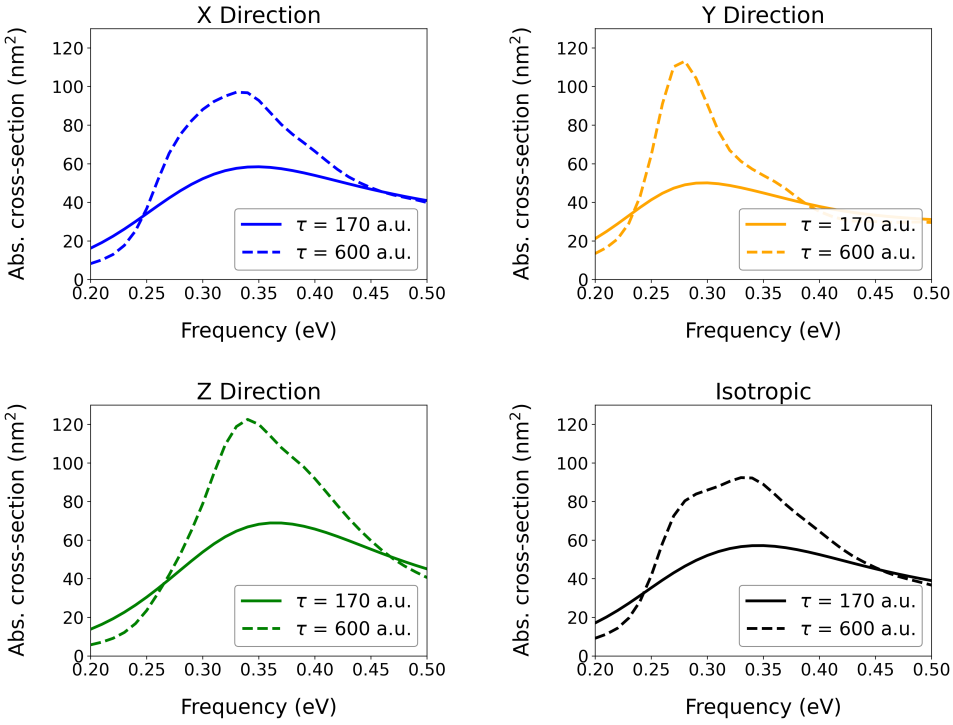

Figure S2: ωFQ absorption spectra of the cured M34-2000 structure (generated from a 50% replication of the unit cell) using $\tau = 170$ a.u. and $\tau = 600$ a.u..

Table S4: Maximum electric field enhancement $|E|/|E_0|$ for the M34-2000 Cured structure (generated from a 50% replication of the unit cell) using $\tau = 170$ a.u. and $\tau = 600$ a.u. as a function of the field polarization.

	Maximum $\|E\|/\|E_0\|$	
Polarization	$\tau = 170$ a.u	$\tau = 600$ a.u
$\vec{E}_x$	25.92	62.92
$\vec{E}_y$	37.73	123.66
$\vec{E}_z$	32.21	119.85
Average	32.09	102.14

S3 Optical Absorption: Cured M34-2000 *vs.* Cured M34-2500

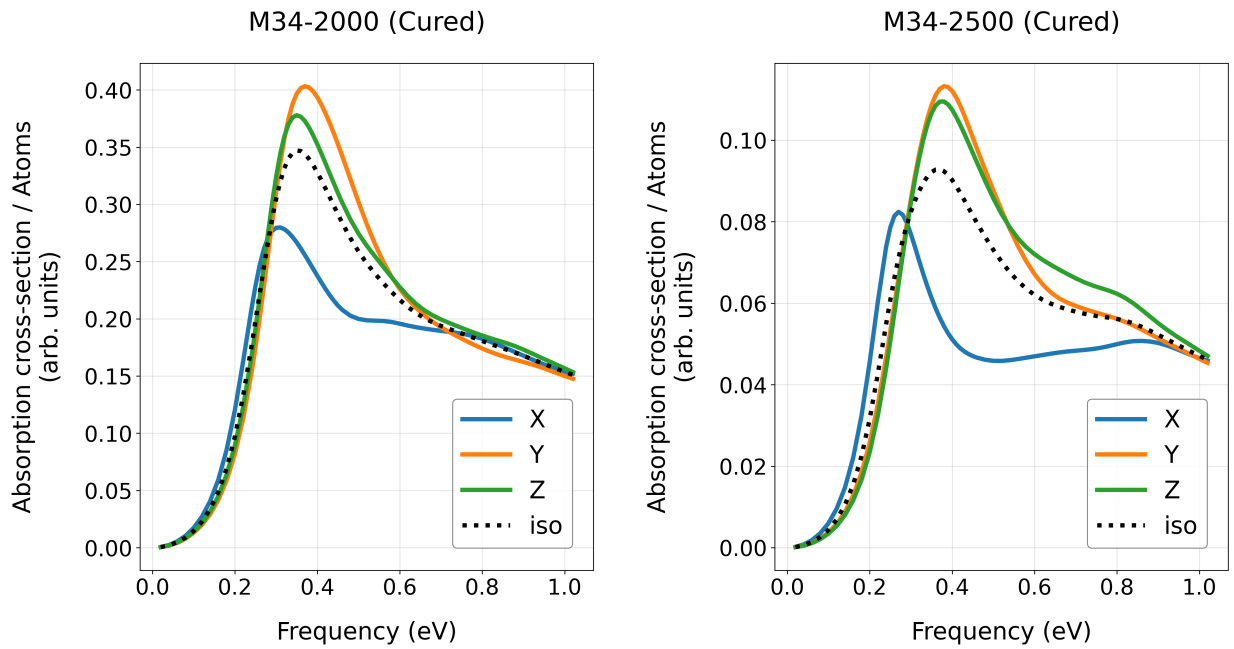

Figure S3: ωFQ absorption spectra of the cured M34-2000 and M34-2500 structures (generated from a 50% replication of the unit cell), normalized by the total number of atoms.

S4 Three-dimensional density

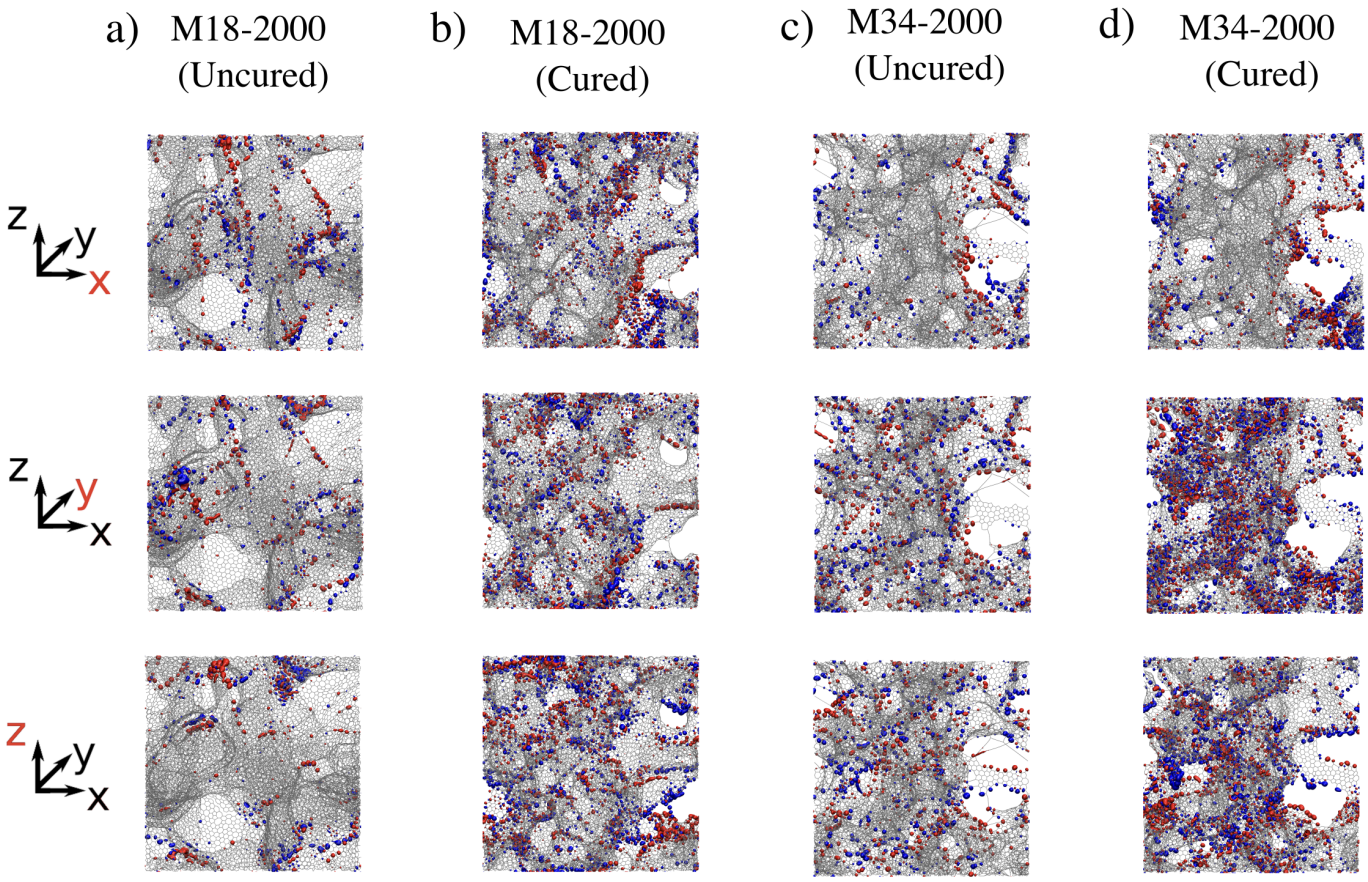

Figure S4: ωFQ induced densities for X, Y, and Z field polarizations for M18-2000 (a-b) and M34-2000 (c-d) in their uncured (a,c) and cured (b,d) forms. The maps are provided within the central unit cell.

S5 Electric field enhancement

S5.1 Effective Volume and Effective Area

Table S5: Effective volume and effective area for M18-2000 and M34-2000 a-C superstructures in their uncured and cured forms as a function of the field polarization calculated on the representative planes shown in Fig. 3 in the main text.

Structure	**Effective volume** ($\times 10^{-2}$ **nm**^{3})				**Effective area** ($\times 10^{-2}$ **nm**^{2})			
	M18-2000		**M34-2000**		**M18-2000**		**M34-2000**	
	Uncured	Cured	Uncured	Cured	Uncured	Cured	Uncured	Cured
$\vec{E}_x$ (YZ plane)	5.682	1.031	3.894	0.841	28.408	5.153	19.469	4.203
$\vec{E}_y$ (XZ plane)	7.692	3.187	8.559	0.786	38.462	15.935	42.796	3.932
$\vec{E}_z$ (XY plane)	6.765	1.954	15.335	4.819	33.824	9.771	76.674	24.096
Average	6.713	2.057	9.263	2.149	33.565	10.286	46.313	10.744

S5.2 2D Field Enhancement Maps

S5.2.1 M18-2000 Uncured

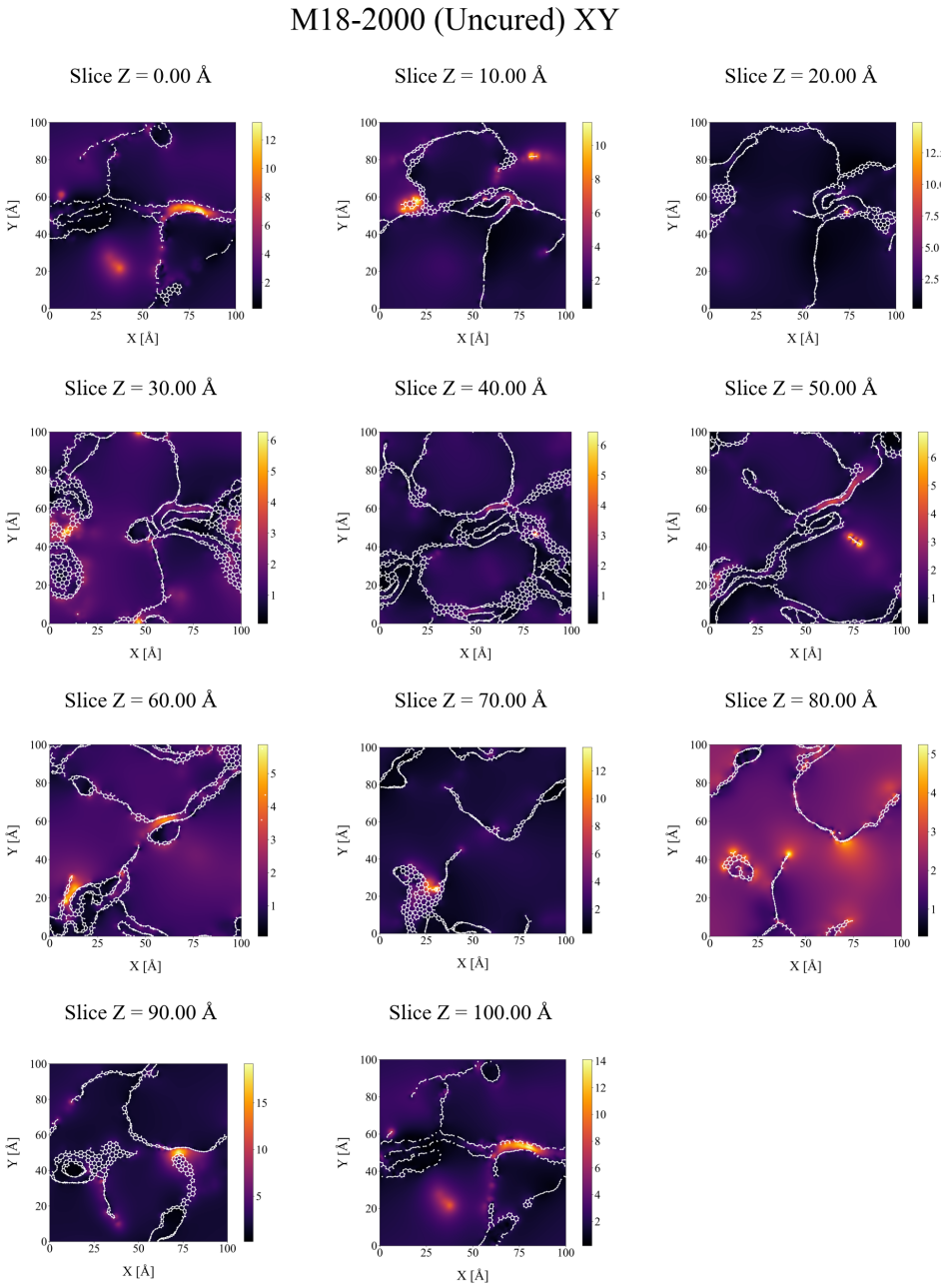

Figure S5: 2D field enhancement maps on XY planes for the uncured M18-2000 structure.

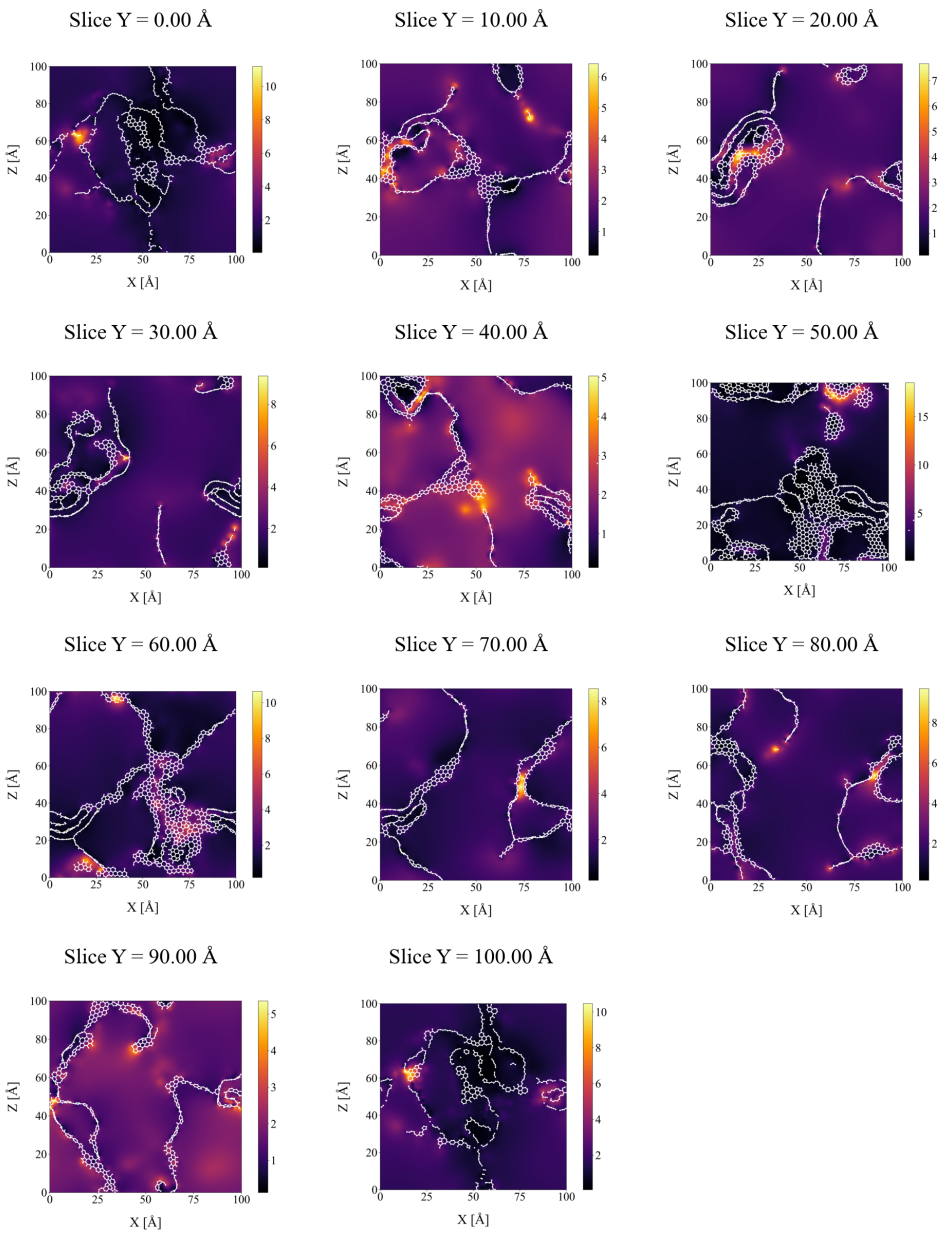

Figure S6: 2D field enhancement maps on XZ planes for the uncured M18-2000 structure.

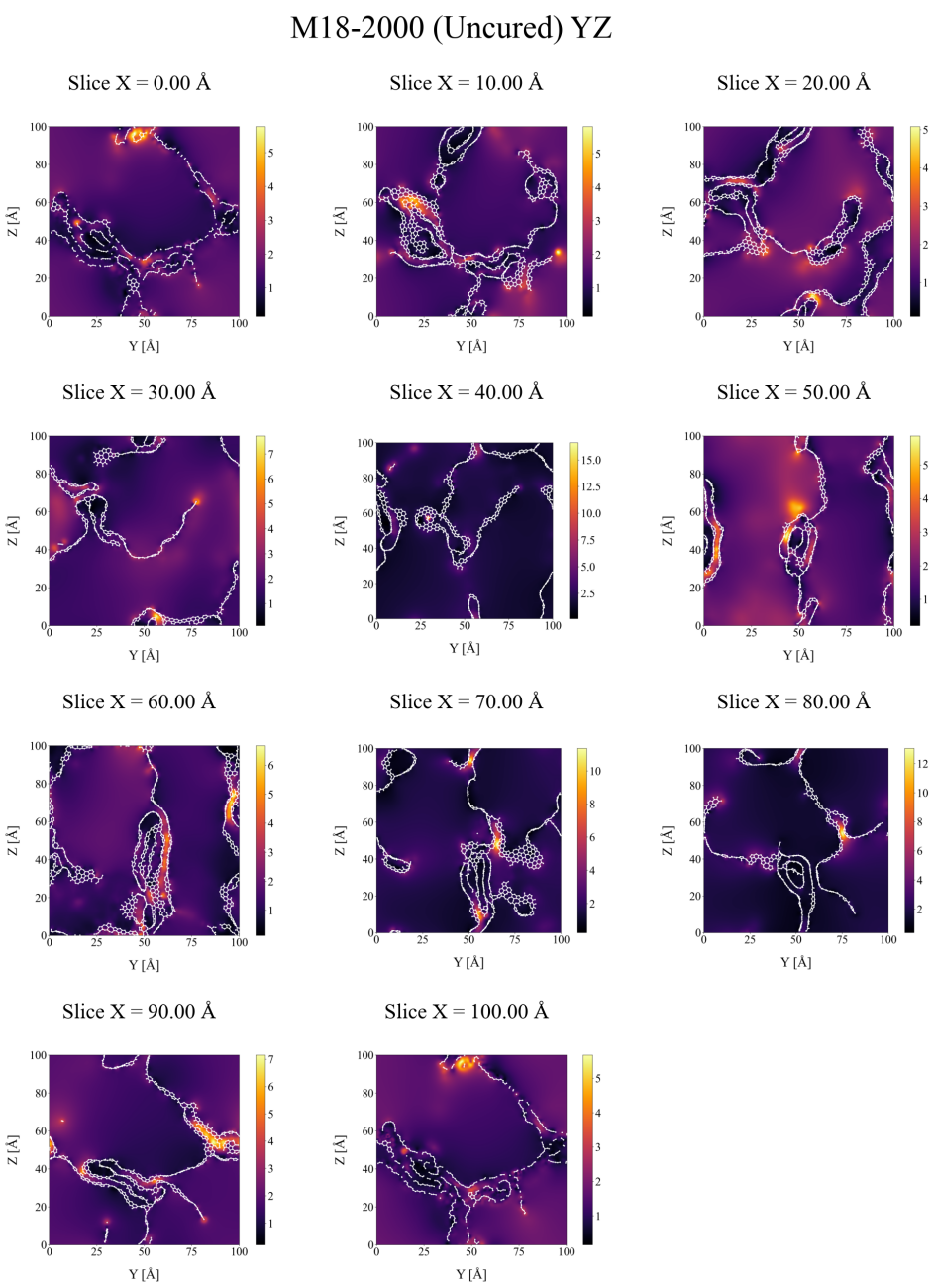

Figure S7: 2D field enhancement maps on YZ planes for the uncured M18-2000 structure.

S5.2.2 M18-2000 Cured

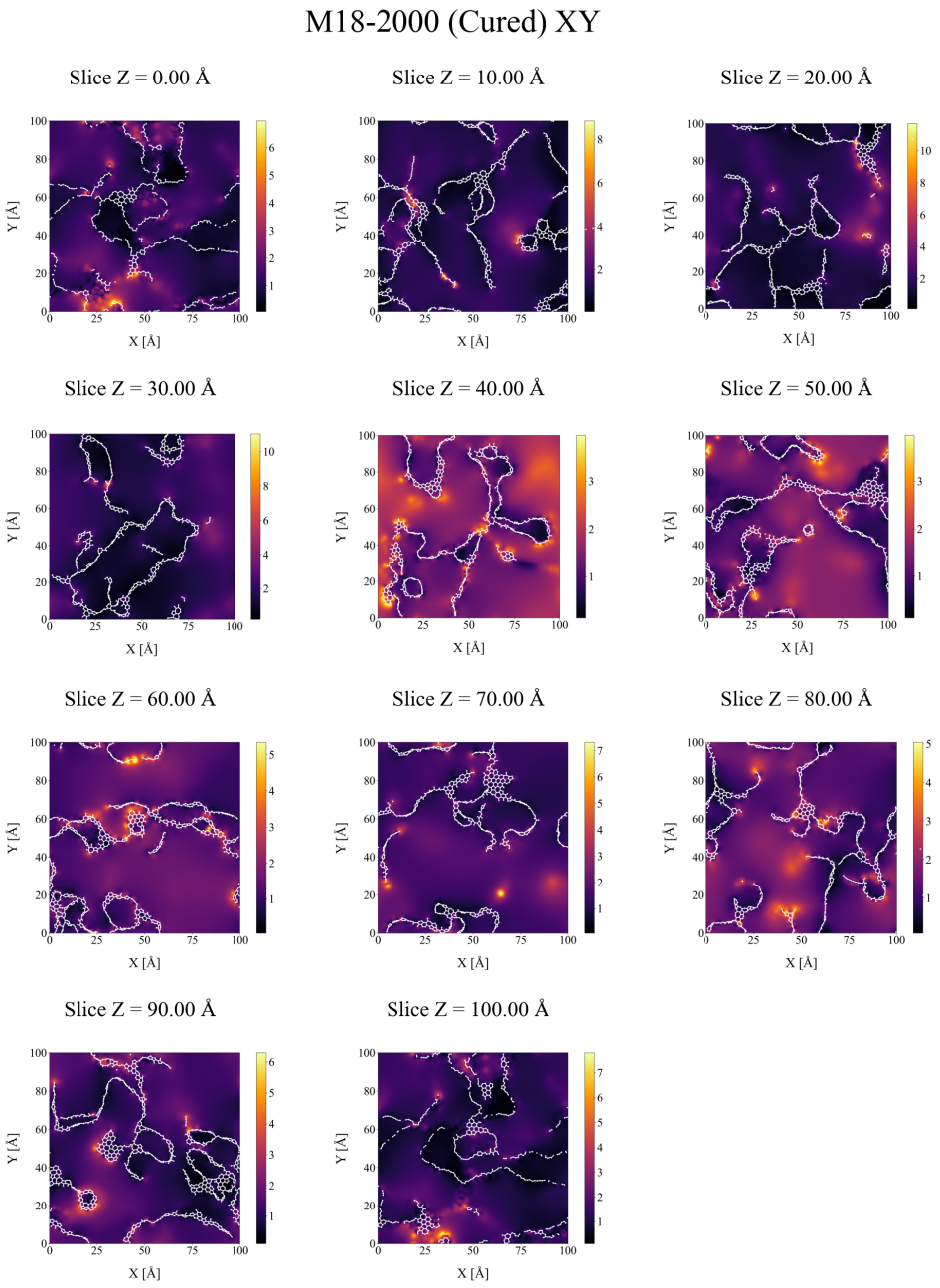

Figure S8: 2D field enhancement maps on XY planes for the cured M18-2000 structure.

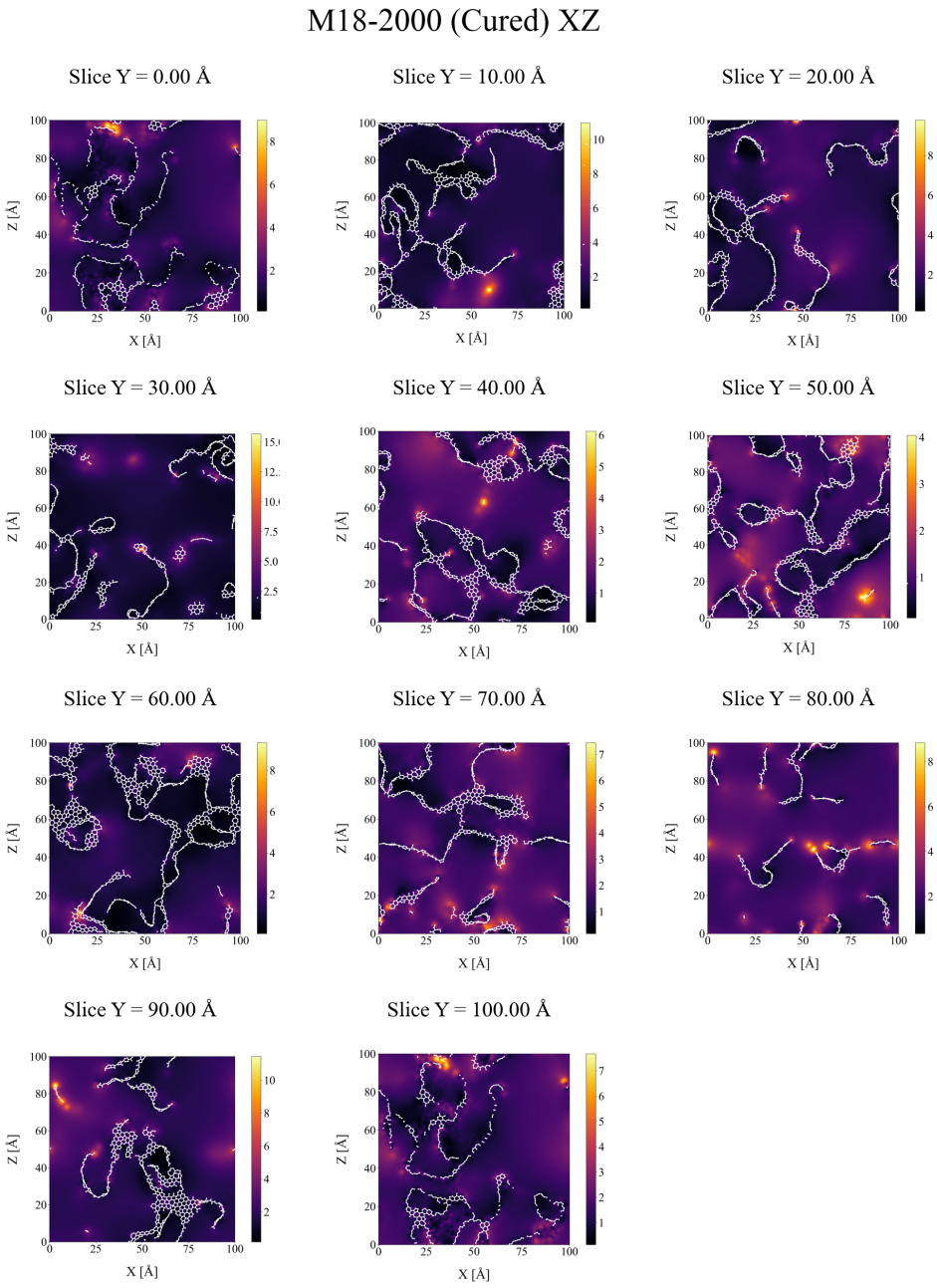

Figure S9: 2D field enhancement maps on XZ planes for the cured M18-2000 structure.

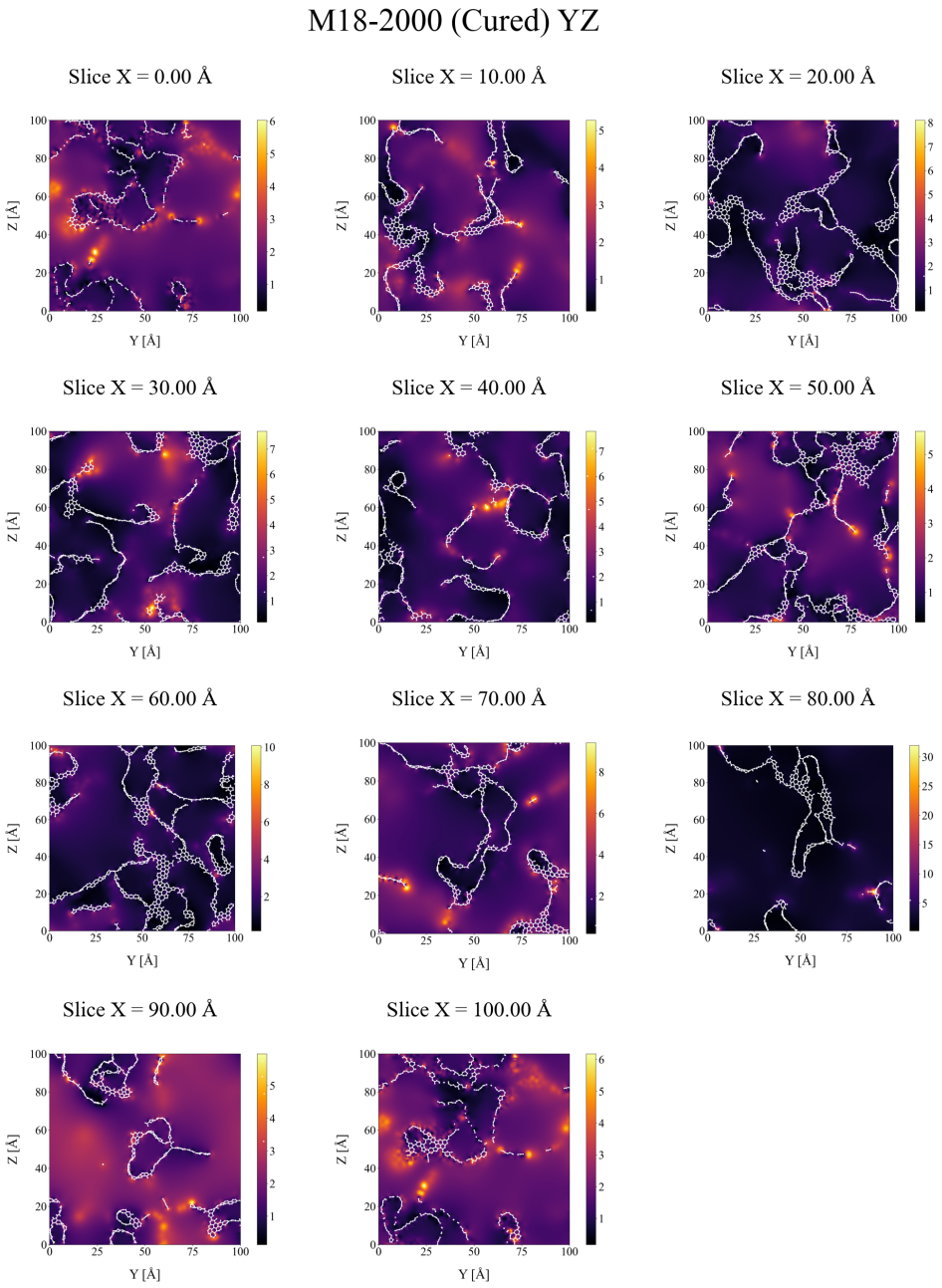

Figure S10: 2D field enhancement maps on YZ planes for the cured M18-2000 structure.

S5.2.3 M34-2000 Uncured

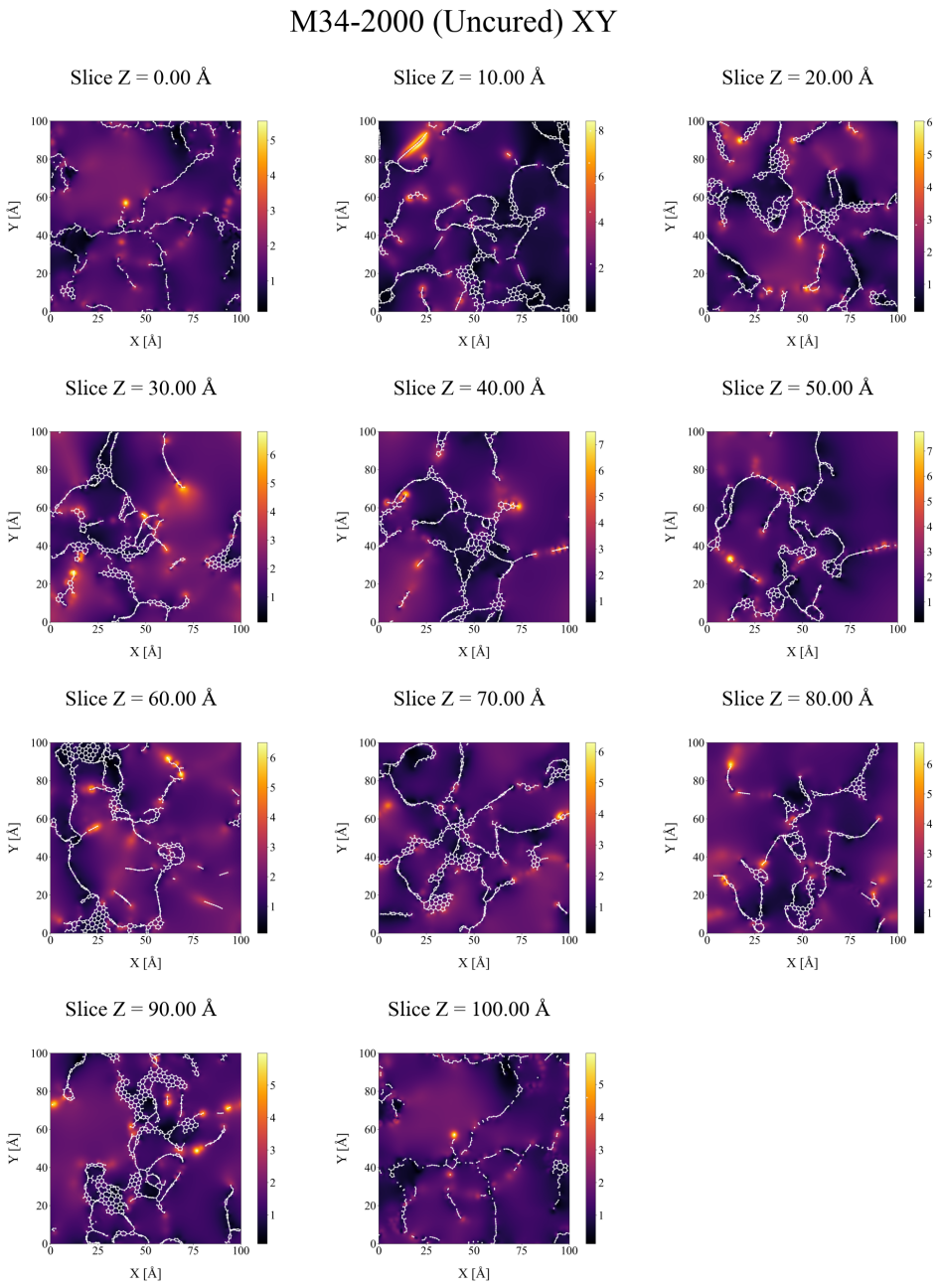

Figure S11: 2D field enhancement maps on XY planes for the uncured M34-2000 structure.

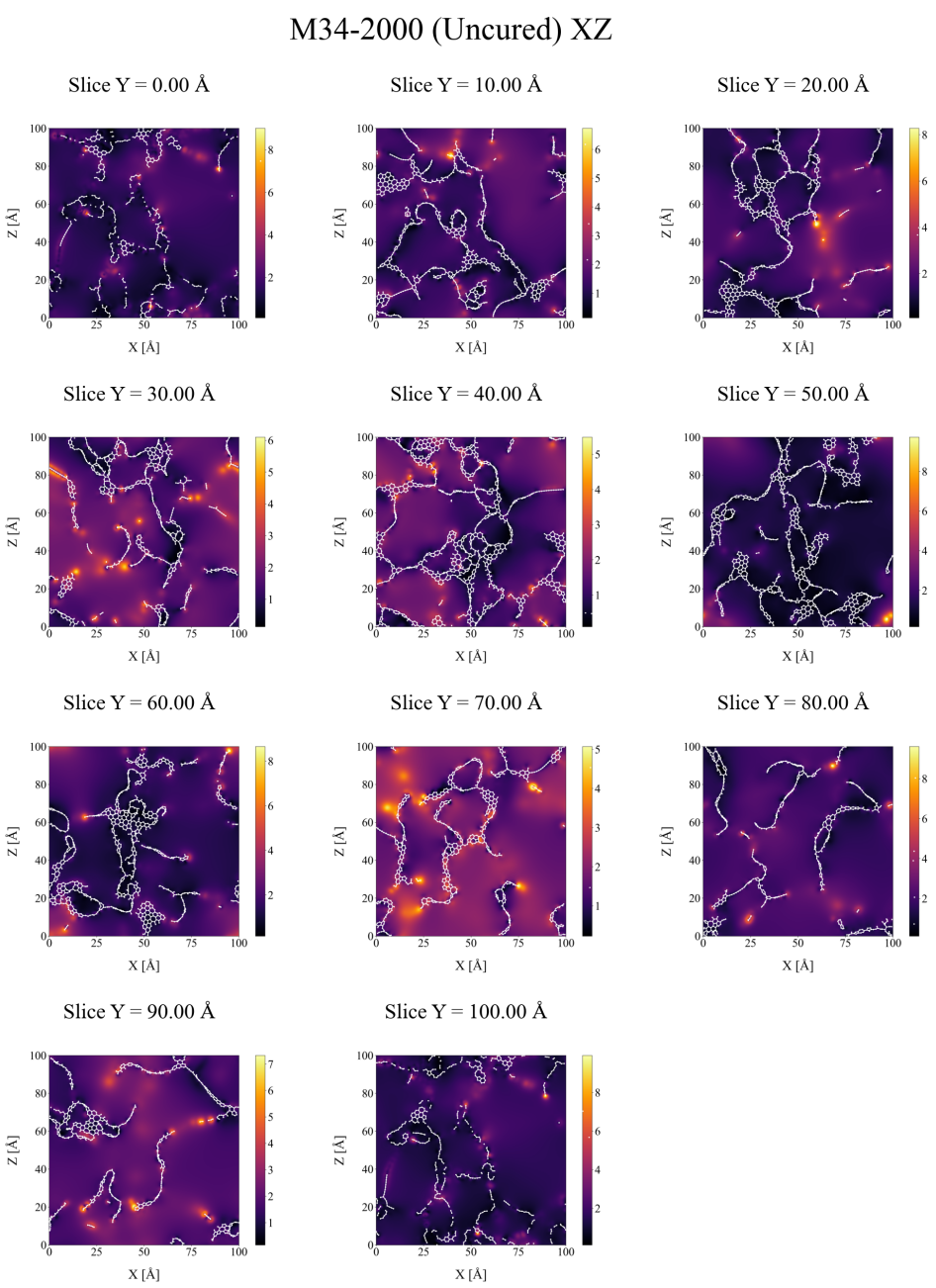

Figure S12: 2D field enhancement maps on XZ planes for the uncured M34-2000 structure.

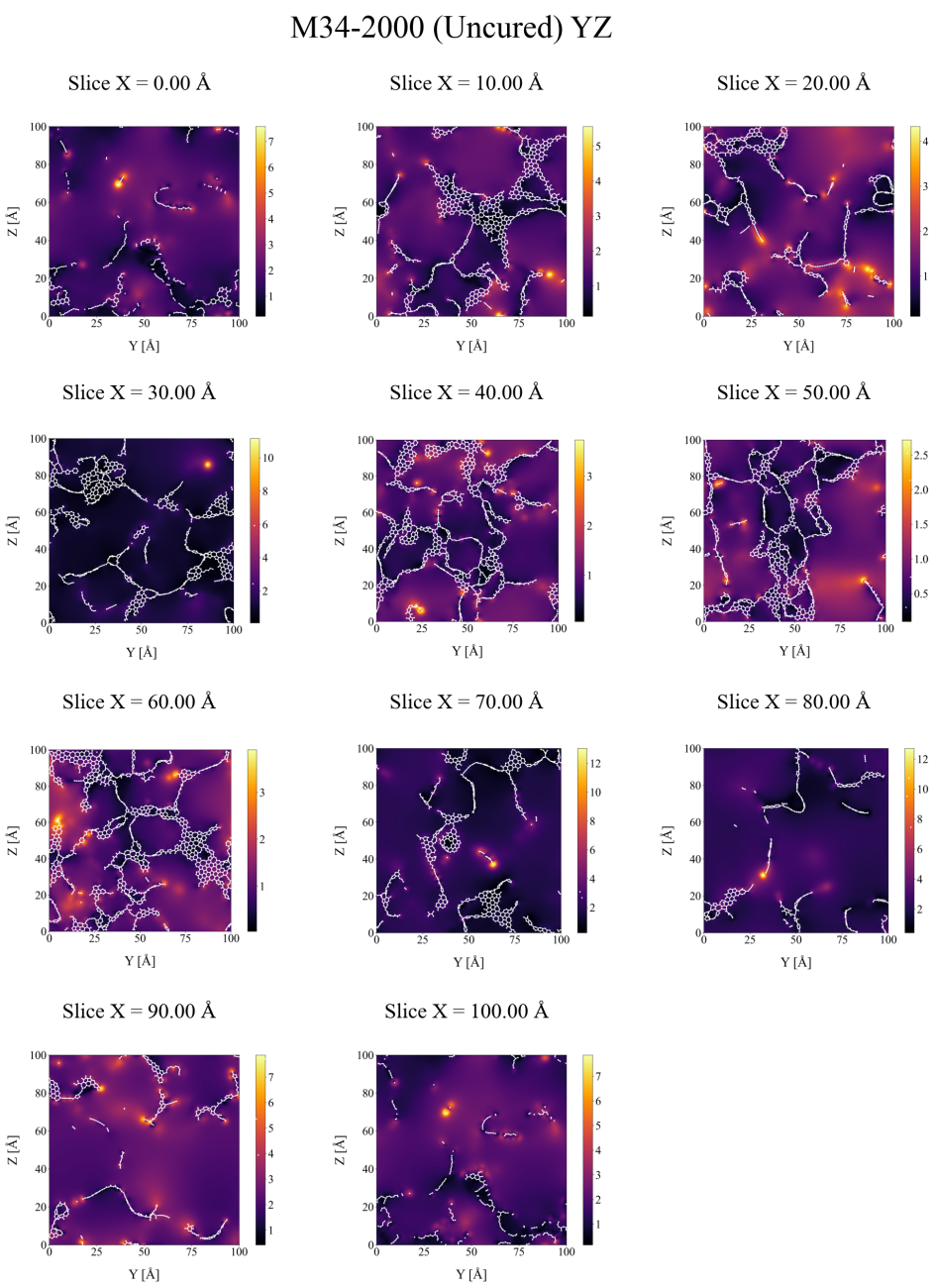

Figure S13: 2D field enhancement maps on YZ planes for the uncured M34-2000 structure.

S5.2.4 M34-2000 Cured

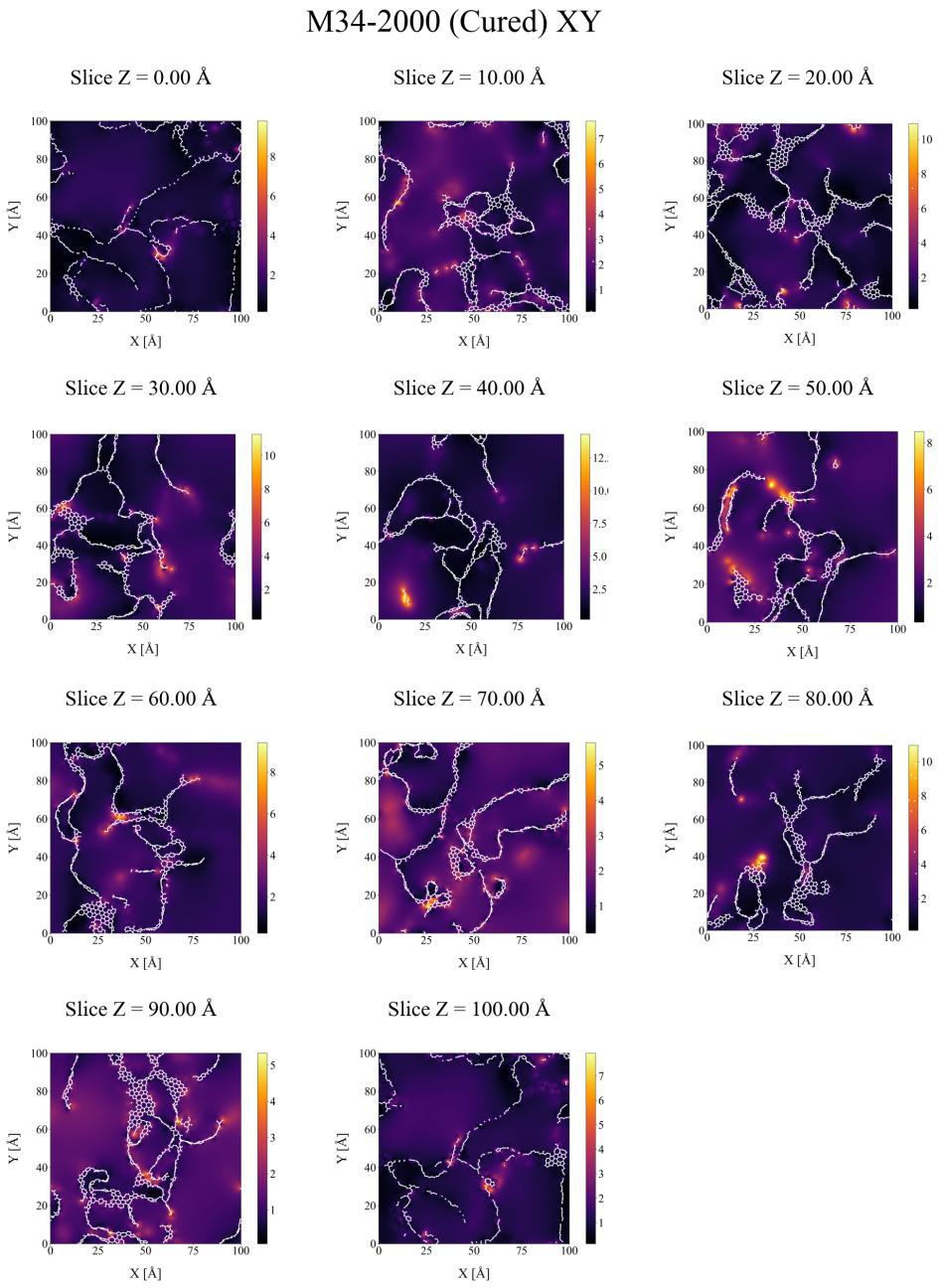

Figure S14: 2D field enhancement maps on XY planes for the cured M34-2000 structure.

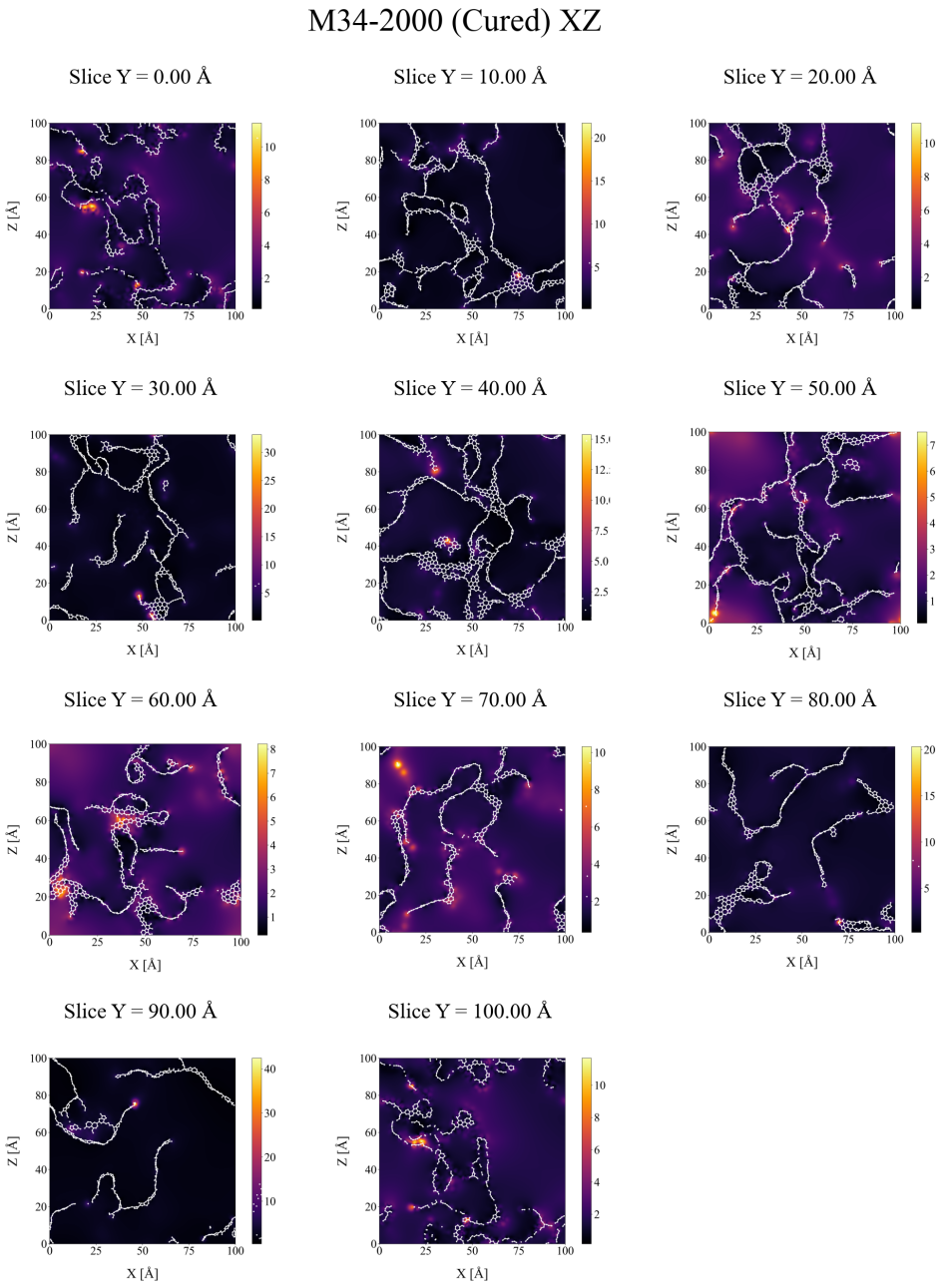

Figure S15: 2D field enhancement maps on XZ planes for the cured M34-2000 structure.

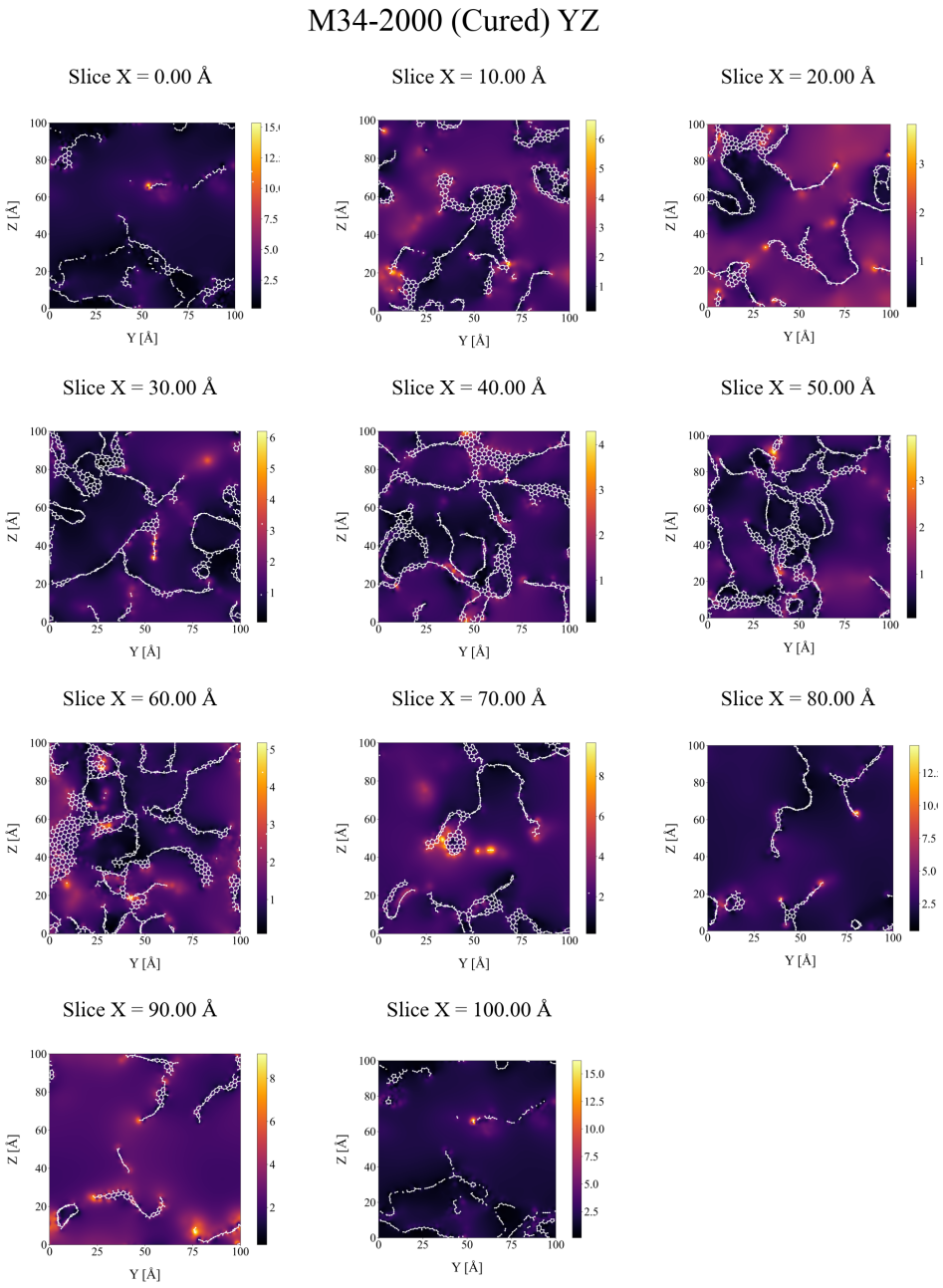

Figure S16: 2D field enhancement maps on YZ planes for the cured M34-2000 structure.

References

(1) Monti, S.; Barcaro, G.; Goddard, W. A. I.; Fortunelli, A. Diverse Phases of Carbonaceous Materials from Stochastic Simulations. *ACS Nano* **2021**, *15*, 6369–6385.

(2) Conter, G.; Monti, S.; Barcaro, G.; Goddard, W. A. I.; Fortunelli, A. Functionalized Amorphous Carbon Materials via Reactive Molecular Dynamics Simulations. *ACS Applied Materials & Interfaces* **2024**, *16*, 48043–48057.

(3) Giovannini, T.; Bonatti, L.; Polini, M.; Cappelli, C. Graphene plasmonics: Fully atomistic approach for realistic structures. *J. Phys. Chem. Lett.* **2020**, *11*, 7595–7602.